© 2010 The Chemical Society of Japan

Selected Papers

Facile One-Step Synthesis of Double-Shelled CeO_2 Hollow Spheres and Their Optical and Catalytic Properties

Jingjing Ma,[1,2] Kun Qian,[1,3] Weixing Huang,*[1,3] Yanhua Zhu,[1,2] and Qing Yang*[1,2]

[1]Nanomaterial and Nanochemistry, Hefei National Laboratory for Physical Sciences at Microscale, University of Science and Technology of China, Hefei, Anhui 230026, P. R. China

[2]Department of Chemistry, University of Science and Technology of China, Hefei, Anhui 230026, P. R. China

[3]Department of Chemical Physics, University of Science and Technology of China, Hefei, Anhui 230026, P. R. China

Received May 19, 2010; E-mail: qyoung@ustc.edu.cn, huangwx@ustc.edu.cn

Double-shelled CeO_2 hollow microspheres (4–5 μm) were synthesized through a facile one-step hydrothermal treatment of $Ce(NO_3)_3 \cdot 6H_2O$ in the presence of citric acid and hexamethylenetetramine (HMTA), and scanning and transmission electron microscopies demonstrated the samples are hollow spheres with litchi-like surfaces. The assembly of the hollow spheres was contributed to coordination effect of additives employed in the reaction system and the ripening growth in the process. Meanwhile, two other spherical structures including polyhedron-constituted and porous microspheres assembled with nanocrystals were also synthesized by varying the experimental parameters in the synthetic route. The UV–vis spectroscopic investigation demonstrated that the absorption edge of the three samples was blue shifted accordingly with their constituted primary crystallite sizes. In addition, investigation showed that the catalytic activities for CO oxidation of the three spheres types were considerably higher than those of commercial CeO_2 powders, and their activities were in the order of porous > litchi-like double-shelled hollow > polyhedron-constituted, consistent with their BET surface area of 33, 22, and 10 $m^2 g^{-1}$. Specially, the litchi-like double-shelled hollow spheres showed much better catalytic properties per unit weight catalyst.

Recently, functional hollow spheres of metal oxide with nanometer- to micrometer-scale dimensions have been receiving much attention due to their wide applications, such as oxygen sensors,[1] drug delivery,[2] protection of sensitive biomolecules,[3] microcapsule microreactors,[4] water treatment,[5] and as a good potential electrode material for photochemical solar cells.[6] Generally, the most common synthetic method involves different templates-directed protocols, typically silica,[7] polymeric beads,[8] or carbon particles[9] which are described as hard templates, and vesicles,[10] emulsions,[11] as well as block copolymer micelles[12] described as soft templates are primarily applied. However, hollow spheres with double-shells have been less reported.[13–15]

Ceria, as a typical type of rare earth oxide, has always been the focus of intense attention since it is widely applied to electronic materials, catalysts, optical and chemical materials, electrolyte materials of solid oxide fuel cells, ultraviolet-blocking materials, and solar cells. Because the properties of rare-earth oxides depend strongly on their size and morphologies, ceria with different shapes and size have been synthesized, for example as nanorods,[16] nanowires,[17] nanotubes,[18] hollow nanocubes,[19] nanosheaves,[20] microplates,[21] and other uncommon shapes including twofold-shaped dendrites,[22] flower-like nanostructures,[23] and spherical structures.[24] In addition, hollow ceria with single shell have also been synthesized by using different hard templates such as carbon spheres,[25,26] carbonaceous polysaccharide spheres,[27] silica spheres,[28] and anionic PSA latex particles.[29] Recently, Yang et al. fabricated CeO_2 hollow microspheres by using a hydrothermal approach.[30] However, to the best of our knowledge, there has been no report on the synthesis of double shell-like ceria-based hollow microspheres. Such a distinct structure of cerium oxide would bring forth new properties, and could be a promising material in desirable chemistry.

Herein, we report a facile hydrothermal process for the formation of the ceria double-shelled hollow spheres with the use of citric acid and HMTA as additives. In the reaction system, HMTA served as a structure-control additive,[31] and citric acid as a pH regulator, and they both could be employed as coordinators, and coordinate with Ce ions to form corresponding complexes in aqueous solution in the current synthetic process. Thus, these as-synthesized complexes are favorable for the assembled aggregation of small nanoparticles, generated at elevated temperatures, to form hollow spheres due to the balance of solution thermodynamics and growth kinetics. This route provides an alternative process for the growth of hollow spherical crystals, and also it is to be noted here that both HMTA and citric acid are economical and environmental-friendly materials and thus of valuable prospect for commercial production. Meanwhile, two other spherical structures including polyhedron-constituted and porous microspheres were also synthesized by varying the experimental parameters in the

Published on the web November 27, 2010; doi:10.1246/bcsj.20100144

system. The three as-synthesized products indicate good UV–vis properties, which are related to their constituted primary crystallite size. The catalytic activity of the three kinds of CeO_2 spheres was probed by CO oxidation. The polyhedron-constituted, litchi-like, and porous structure CeO_2 spheres are much more catalytically active than commercial CeO_2 powder, and the litchi-like double-shelled hollow product exhibits the highest specific catalytic reaction rate, demonstrating that it has the best redox behavior.

Experimental

Materials. Cerium nitrate ($Ce(NO_3)_3 \cdot 6H_2O$, ≥99.0%), citric acid ($C_6H_8O_7 \cdot H_2O$, Analytical reagent (A. R.) grade), and hexamethylenetetramine (=1,3,5,7-tetraazatricyclo-[3.3.1.$1^{3,7}$]decane, HMTA, $(CH_2)_6N_4$, A. R. grade) were purchased from National Chemical Reagent Cooperation Ltd., Shanghai, and used without further purification.

Synthesis of Litchi-Like Double-Shelled Hollow Spheres. In a typical synthesis, $Ce(NO_3)_3 \cdot 6H_2O$ (2.0 mmol) and HMTA (0.75 mmol) were dissolved in deionized water (20 mL) with magnetic stirring, then citric acid (1.0 mmol) was added, forming a transparent solution with pH 2.3. This solution was stirred for about 1 h and then transferred into a 30 mL Teflon-lined autoclave which was sealed and kept at 195 °C for 20 h. After the autoclave was cooled to room temperature naturally, precipitation was separated by centrifugation, washed with deionized water and absolute alcohol several times and dried in an oven at 60 °C overnight.

Characterization. The phase purities of the products were characterized by X-ray diffraction (XRD) performed on a Philips X'Pert diffractometer with graphite-monochromatized Cu Kα radiation ($\lambda = 1.54178$ Å) at a scanning rate of 0.02 degree s^{-1} in the 2θ range from 10 to 70°. The surface morphology of the samples was observed by scanning electron microscopy (SEM, S-4800, Hitachi Co., Japan). Transmission electron microscopy (TEM) images and high-resolution TEM (HRTEM) images were obtained on a JEOL-2010 with an accelerating voltage of 200 kV. X-ray photoelectron spectroscopy (XPS) measurements were carried out on a VGESCALAB MKII X-ray photoelectron spectrometer with an exciting source of Al Kα. The UV–vis diffuse reflectance spectroscopy (DRS) was performed on a Hitachi U-4100 UV–vis–NIR spectrophotometer with the integration sphere diffuse reflectance attachment. The Brunauer–Emmett–Teller (BET) tests were performed with a Micromeritics ASAP-2000 nitrogen adsorption apparatus. The catalytic activity for CO oxidation was measured with a continuous flow reactor at atmospheric pressure and a gas mixture (1 vol % CO, 99 vol % air) was fed at a flow rate of 20 mL min^{-1} to the reactor which contained 30 mg samples.

Results and Discussion

Characterizations of Typical Sample. The phase purity and crystallinity of the as-synthesized CeO_2 sample were investigated by XRD. All of the diffraction peaks shown in Figure 1 indicate the good crystallization of the sample and can be exactly indexed as a pure face-centered cubic phase [space group: $Fm\bar{3}m$ (No. 225)] with lattice constant $a = 5.412$ Å, which is consistent with the value of standard card (JCPDS 81-0792). Based on the Scherrer equation, the average crystallite size is about 37.3 nm in diameter for the sample, evaluated via the calculation of the half-width of the (111) diffraction peak.

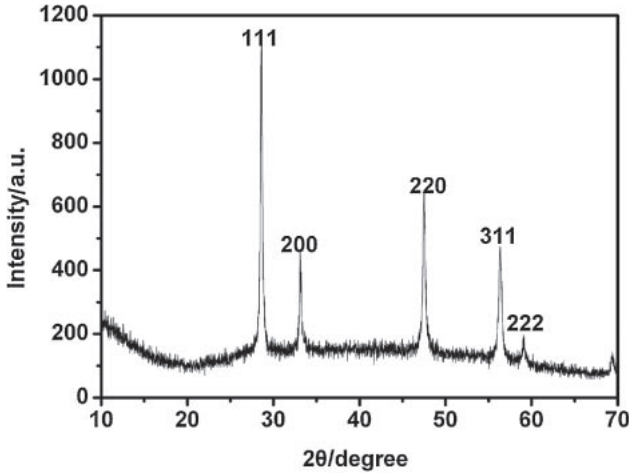

Figure 1. XRD pattern of the product obtained at 195 °C for 20 h in a typical synthesis.

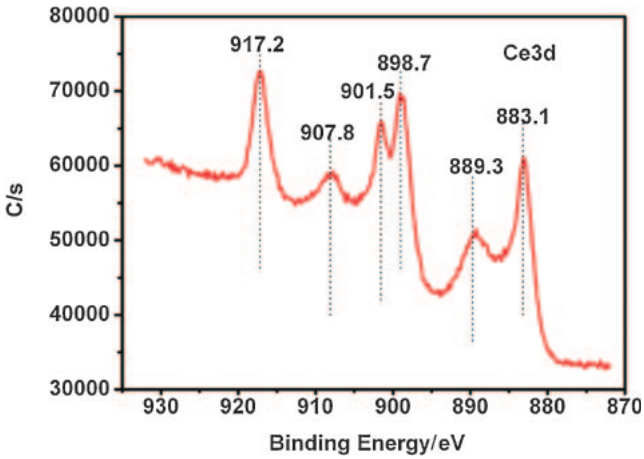

Figure 2. XPS spectrum of an as-synthesized ceria sample.

The oxidation state of Ce in ceria can be examined by XPS (Figure 2), the six Ce3d binding energy peaks corresponded to a previous report of Ce(IV),[32] suggesting the valence of cerium in the typical system was +4. The binding energy at 883.1, 889.3, and 898.7 eV are attributed to Ce $3d_{5/2}$, and 901.5, 907.8, and 917.2 eV are signed to Ce $3d_{3/2}$. Therefore, the XPS investigation further confirmed the chemical formula of the as-synthesized sample is CeO_2.

The morphologies of the product were characterized by SEM and TEM. Figures 3a and 3b show some typical SEM images of double-shelled CeO_2 spheres. The low-magnification image (Figure 3a) shows that the as-prepared CeO_2 product is mainly composed of spheres with a mean diameter of 4–5 μm with hollow interiors, which can be seen from the broken ones. The high-magnification image (Figure 3b) shows that most of the spheres were largely made up of two layer structured shells with litchi-like surfaces. A typical TEM image of the hollow spheres is shown in Figure 3c, there was a clear hollow center with shell thickness of about 300 nm which is featured by the apparent distinction between the dark edge and light center,

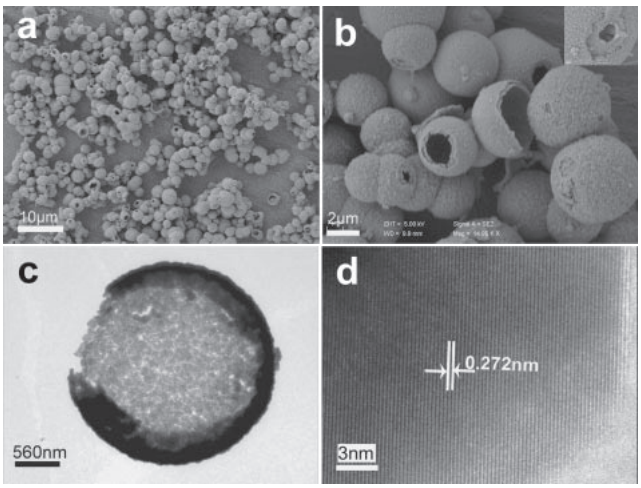

Figure 3. SEM images of double-shelled CeO_2 microspheres: (a) low magnification and (b) high magnification of double-shelled CeO_2 spheres, (c) TEM image of a single CeO_2 hollow microsphere, and (d) HRTEM image of the CeO_2 product.

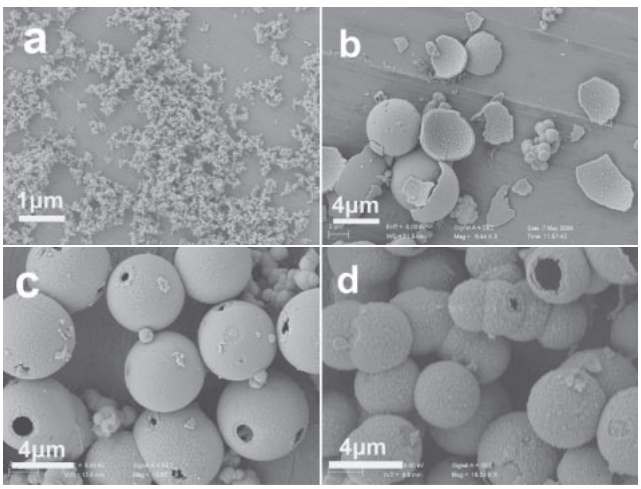

Figure 4. SEM images recorded during the different reaction times of the two-layer structures: (a) 1, (b) 3, (c) 6, and (d) 20 h.

while the double shells were not clearly observed possibly because the two shells are very close. Obviously, the hollow spheres are assembled by nanostructured crystals of about 30 nm in diameter. Figure 3d exhibits a HRTEM image for the product with interplanar spacing of 0.272 nm, indicating that the assembled nanocrystals within the spheres show single-crystal nature.

Formation Mechanism. To understand the growth mechanism of the double-shelled hollow spheres, a set of time-dependent experiments were carried out. The SEM images of the products obtained at varied reaction times are shown in Figure 4. It is noted that the product collected at 1 h (Figure 4a) mainly consists of random distributed small nanocrystals. When the reaction time was extended to 3 h, some small CeO_2 nanocrystals assembled into regular spheres with a larger diameter of about 4–5 μm, and the assembled spheres appeared with thin layers while most of the spheres would crack into fragments as shown in Figure 4b. When reaction time was further prolonged to 6 h, the thin-shelled hollow spheres structure grew thick and the fragments could not be observed in samples, still, there were some small particles of about 500 nm mixed with the spheres. After reaction of 20 h, the small particles disappeared thoroughly via ripening growth and single-shelled structures translated into double-shelled entirely and the microspheres present with litchi-like surfaces, as shown in Figure 4d.

On the basis of the above investigation, an assembly growth model can be proposed for the double-shelled hollow spheres. The formation of CeO_2 involves the following steps: that is, Ce(III) first coordinated with citric acid forming stabilized complex cerium citrate (Ce(III)–citrate), and then at elevated temperatures, HMTA decomposed to formaldehyde and ammonia through acid hydrolyses due to its relatively low decomposition temperature compared with citrate acid. No doubt Ce(III)–citrate decomposed in the same process over prolonged time. Meanwhile, CeO_2 was synthesized via the oxidation of Ce(III) with oxygen involved in the reaction system under the equilibrium between coordination and decomposition of citric acid, which would be favorable for the assembly of the double-shelled spheres. The main reactions involved in the reaction system could be illustrated as follows:

$$Ce^{3+} + HO\text{—}C(CH_2\text{—}COOH)_2 \rightarrow HO\text{—}C(CH_2\text{—}COO)_2\text{—}Ce - 3H^+ \quad (1)$$

$$HMTA - H_3O^- \rightarrow NH_4^+ + HCHO \quad (2)$$

$$HO\text{—}C(CH_2\text{—}COO)_2\text{—}Ce + O_2 \rightarrow CeO_2 - CO_2 + H_2O \quad (3)$$

It is noted here that citric acid is used as a pH regulator and capping agent,[33] and HMTA as a structure-control additive,[31] and they both play important roles in the formation of CeO_2 spheres. Generally, citric acid is of spatial structure and it can coordinate with central metal ions to form metal complexes with a centrosymmetric[34] or a disordered structure,[35] although the structures of rare earth citrates are not well documented,[36] in which the citric root can be seen as a tie or bond between the nanocrystals for the assemblies of these nanocrystals. Previously, ceria nanoparticles were hydrothermally obtained in the presence of citric acid at 180 °C for 24 h,[37] however, there were not any regular assemblies achieved without the use of HMTA. Similarly, we could not obtain spherical assemblies either at the absence of HMTA via a number of experiments. So, the effect of HMTA cannot be ignored in the present process. As we know, HMTA as a water-soluble, nonionic tetradentate cyclic tertiary amine can also act with Ce ions in aqueous solution even though the Ce–HMTA complex was not reported previously. Based on hard–soft acid–base theory, the action between Ce ions and nitrogen atom from HMTA is weaker than

Table 1. Reaction Conditions of the Three Types of CeO_2 Samples (20 h)

$Ce(NO_3)_3 \cdot 6H_2O$ /mmol	HMTA /mmol	Citric acid /mmol	Stirring temperature /°C	Reaction temperature /°C	Products morphology
2.0	0.75	1.0	20	195	litchi-like double-shelled hollow spheres
1.5	0.75	0.5	20	220	porous spheres
1.0	0.125	0.5	100	220	polyhedron-constituted spheres

that of oxygen within citric acid. As a sequence, there will be a balance or equilibrium between the two coordinative reactions of the Ce ions with the two ligands. So at the initial reaction stage, both the carboxy group of citric acid and the amine of HMTA would coordinate with cerium ion to form their corresponding Ce(III) complexes, of which cerium citrate was stable in a wide range of temperatures kinetically in the process while Ce–HMTA comparatively unstable. Meanwhile, it is noted that HMTA can also connect to the citric acid by hydrogen bond[38] to enhance the steric hindrance which was also favorable for the assembled growth of nanocrystals with spherical shapes.[33] Almost at the same time, Ce(III) was oxidized to CeO_2 in the reaction system accordingly accompanied by the assembly of spheres at elevated temperatures with reaction time prolonged above 3 h (Figures 4b–4d).

It is concluded that the formation mechanisms of the double-shelled hollow spheres should be mainly attributed to self-assembly through the balance between thermodynamics and kinetics in the system. In detail, low-temperature molecule coordinated complexes lead to the assembled aggregation of small nanoparticles generated at elevated temperature via Brownian motion,[19] to form hollow spheres in the presence of HMTA as a structure-control additive.[33] In the initial stage, the aggregated hollow spheres grew with rather coarse surfaces kinetically, and interestingly, most hollow spheres produced in this stage showed incomplete shapes (Figure 4b), since the layer was thin and thus the spheres crack into fragments easily which can be seen from Figure 4b. With the reaction time is prolonged, the broken spheres cannot be observed with the thick layer, and at the same time the shell of the spheres would rearrange from one thin shell spheres to double thick spheres via long time mass transfer during growth. As a result, the double-shelled hollow spheres with smooth surface were acquired due to the mass transfer under the conditions between the balances of thermodynamics and kinetics in the current coordinative system. In other words, both citric acid and HMTA act with Ce ions to form their corresponding complexes. The two complexes possess different complexation constants, space effects, and thermal stability, and these variations between the two complexes result in the dynamic balance of complexation, dissociation between the complexes, and the nucleation and growth of crystals at about 200 °C for 20 h, which lead to the assembly of hollow spherical structures under the conditions of thermodynamic and kinetic regime.

The XRD pattern in Figure 5 shows the as-prepared porous surface and polyhedron-constituted sphere samples listed in Table 1 are pure CeO_2. Based on the Scherrer equation, the average crystallite size is about 60.7 nm in diameter for

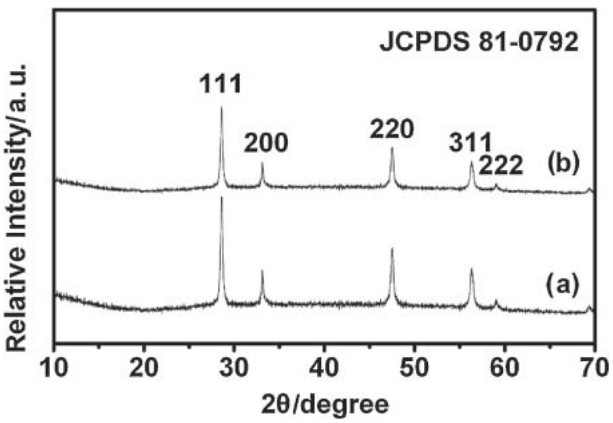

Figure 5. XRD patterns of different surface shape: (a) porous surface and (b) polyhedron-constituted microspheres.

porous sample (Figure 5a), 30.3 nm for polyhedron-constituted (Figure 5b), and 37.3 nm for litchi-like microspheres (Figure 1), respectively, evaluated via the calculation of the half-width of the (111) diffraction peak.

Figure 6a shows the SEM image of the previously mentioned double-shelled CeO_2 hollow spheres with litchi-like surface. The high-magnification SEM image of a single sphere in Figure 6b shows the surface of the sphere was made up of extremely small crystals, which were close-pack arrayed to form a litchi-like structure on the surface. Figure 6c exhibits the SEM image of the porous CeO_2 spheres, with a uniform diameter of 2–3 μm. Likewise, Figure 6d depicts the high-magnification SEM of a single sphere. Clearly, the surface of the spheres was full of broken holes, and some holes broken under the surface, which is similar to skeleton structure. Figure 6e reveals the SEM image of the 2.5 μm polyhedron-constituted CeO_2 and the high-magnification SEM of the surface are shown in Figure 6f. Obviously, a whole sphere consisted of innumerable close-arranged polyhedrons. It is possible that as the citric acid decreased relatively and thus the "bond or tie" reduced in the solution, only a relatively loose structure with multiple holes in the whole spheres is formed ultimately. Likewise, a relatively dense litchi-like microsphere is synthesized as the proportion of citric acid is increased. In addition, the formation of polyhedron-constituted material is mainly attributed to the heating under stirring, which intensifies the nucleation step in comparison with the process without calefaction.

Properties of the Three Samples in the System. Figure 7 presents the UV–vis absorption spectra for the three as-

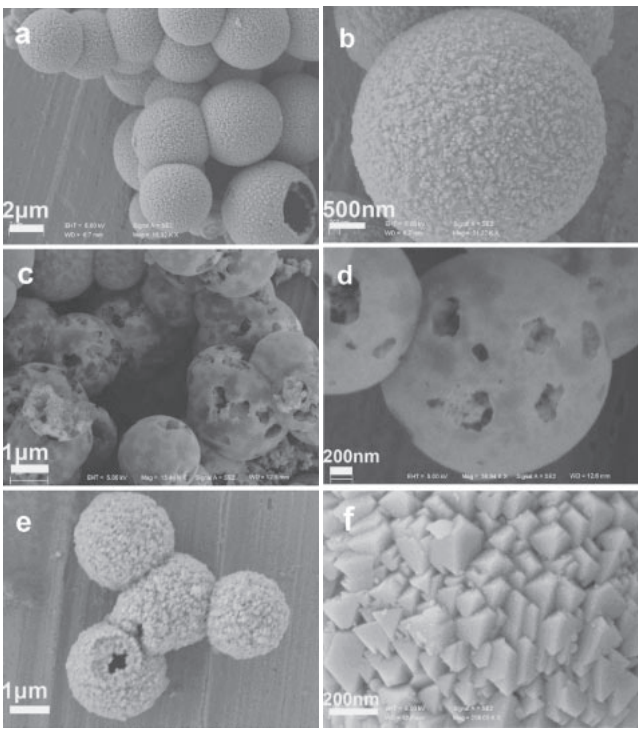

Figure 6. SEM images of microspheres with different structure: (a) low magnification and (b) high magnification of litchi-like double-shelled hollow CeO_2 microspheres, (c) low magnification and (d) high magnification of porous microspheres, (e) the image of the polyhedron-constituted CeO_2, and (f) the corresponding detailed surface shape.

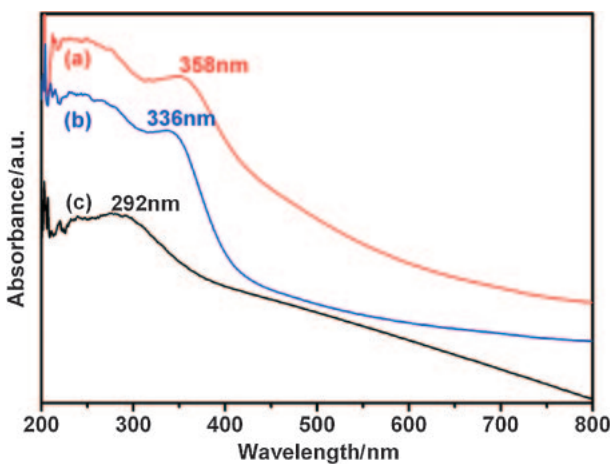

Figure 7. UV–vis absorption spectra of the three CeO_2 microspheres: (a) polyhedron-constituted, (b) litchi-like double-shelled hollow microspheres, and (c) porous ones.

prepared CeO_2 powders in the system. It is revealed that the onsets of the strong absorption edges located at 358, 336, and 292 nm for the polyhedron-constituted, double-shelled, and porous spheres, respectively. They all shifted to lower wavelength in the spectra comparing with the bulk material, which are induced by charge-transfer transition from O^{2-} (2p) to Ce^{4+} (4f) orbital in CeO_2.[39] Considering CeO_2 as a direct band gap semiconductor, the decrease in particle size leads to the blue shift of absorption peak.[40] According to XRD calculation, the

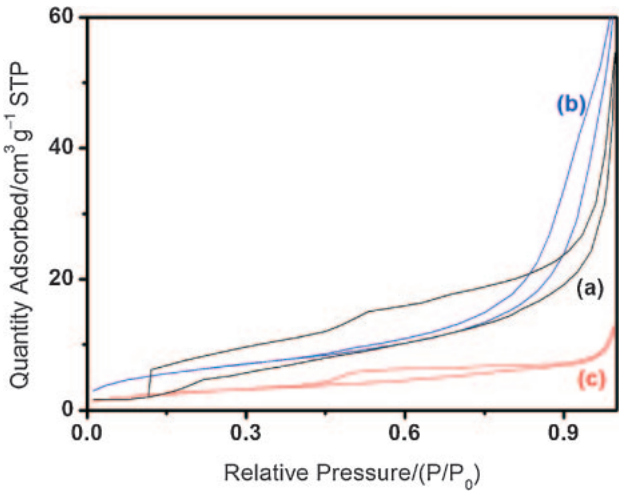

Figure 8. Nitrogen adsorption–desorption isotherms of the three kinds of CeO_2 microspheres: (a) porous CeO_2 microspheres (dark line), (b) double-shelled litchi-like CeO_2 microspheres (blue line), and (c) polyhedron-constituted CeO_2 microspheres (red line).

particle size reduced in the order porous > litchi-like double-shelled > polyhedron-constituted spheres. It can be seen that there is a blue shift in the spectrum from polyhedron-constituted to litchi-like double-shelled, and then to porous spheres.

Figure 8 presents the nitrogen adsorption–desorption isotherms of the three kinds of the CeO_2 spheres. The adsorption and desorption isotherms for the three kinds of spherical structure shows a H_2-type hysteresis loop. The BET specific surface area of the three samples (Figures 8a–8c) was calculated to be 33, 22, and 10 $m^2 g^{-1}$ for porous, double-shelled, and polyhedron-constituted CeO_2 spheres, respectively. It is reasonable that the porous CeO_2 with rich pore structures displays the largest BET surface area whereas the polyhedron-constituted CeO_2 spheres with the close-packed structure shows the lowest BET surface area.

CeO_2 has nice redox behavior because of the existence of a Ce(III)/Ce(IV) redox cycle and thus has been widely applied as the catalyst component for catalytic oxidation reactions. CeO_2 is a key component in the three-way catalyst used for automotive exhaust gas conversion in which CO oxidation is one of the main catalytic reactions. Therefore, the catalytic activity of CeO_2 spheres with different surface shapes in CO oxidation was evaluated. Figure 9a shows the activity of commercial CeO_2 powders. Figures 9b–9d displays the activity of porous, litchi-like, and polyhedron-constituted CeO_2 spheres, respectively. As shown in Figure 9, the CO conversion increased with increasing reaction temperature for all of the samples, and the as-prepared CeO_2 spheres showed a higher catalytic activity than nanoparticles. Generally, the sequence of catalytic activity is the order of porous > double-shelled > polyhedron-constituted spheres, which is in accordance with their BET surface areas. The specific reaction rates shown in Figure 10 demonstrate that the litchi-like double-shelled CeO_2 spheres exhibit the highest specific reaction rate. It is generally accepted that CO oxidation under stationary conditions over ceria follows the Mars–van Krevelen-type mechanism, where

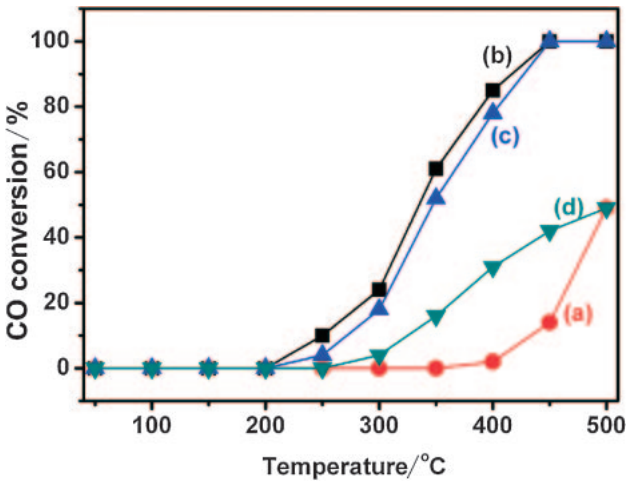

Figure 9. CO conversion images in the presence of CeO_2: (a) the commercial CeO_2 powders (circle red line), (b) porous CeO_2 microspheres (square black line), (c) litchi-like double-shelled CeO_2 microspheres (uptriangle blue line), and (d) polyhedron-constituted CeO_2 microspheres (down-triangle dark cyan line).

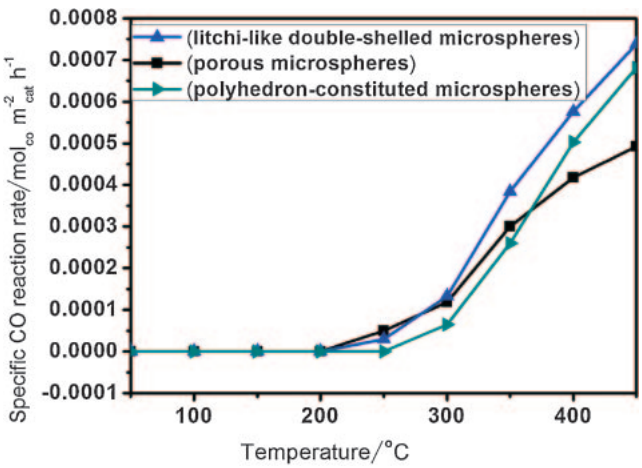

Figure 10. Specific reaction rates of CO oxidation catalyzed by various CeO_2 catalysts.

reaction involves alternate reduction and oxidation of the oxide surface with formation of surface oxygen vacancies (as the key step) and their replenishment by gas-phase oxygen.[41] Therefore, the litchi-like double-shelled CeO_2 spheres should have a better redox behavior than porous and polyhedron-constituted CeO_2 spheres that could be related to their morphology and structure. These results suggest that the reducibility and catalytic activity of CeO_2 catalysts can be tailored more or less by means of morphology control.

Conclusion

In conclusion, the litchi-like double-shelled CeO_2 hollow spheres were synthesized through a facile one-step hydrothermal oxidation of cerium nitrate in the presence of citric acid and HMTA at 195 °C for 20 h, and two other morphologies were also acquired in the system with the variation of reaction conditions. The formation mechanism of the double-shelled hollow CeO_2 spheres is mainly attributed to aggregation and assembly of the preformed nanocrystals. The UV–vis properties of the three morphologies are related to their primary constituted crystal size, and the CO catalytic activity of three samples is excellent compared to commercial CeO_2 powders, and the litchi-like double-shelled hollow spheres show superior catalytic properties. This work provides a convenient, one-step method for the synthesis of the double-shelled hollow spheres, which showed considerably higher catalytic conversion of carbon monoxide to carbon dioxide than those of commercial CeO_2 powders. Specially, the litchi-like double-shelled hollow spheres showed superior catalytic properties per unit weight than other spheres did in the catalytic process.

We gratefully acknowledge the financial support from the National Natural Science Foundation of China (No. 21071136), the National Basic Research Program of China (No. 2010CB934700), the Program for New Century Excellent Talents at Universities from the Chinese Ministry of Education (No. NCET2006-0552), and the Foundation of Anhui Provincial Education Department (No. KJ2008A071).

References

1 a) M. Batzill, U. Diebold, *Phys. Chem. Chem. Phys.* **2007**, *9*, 2307. b) L. Liao, H. X. Mai, Q. Yuan, H. B. Lu, J. C. Li, C. Liu, C. H. Yan, Z. X. Shen, T. Yu, *J. Phys. Chem. C* **2008**, *112*, 9061.

2 a) Y. Bae, S. Fukushima, A. Harada, K. Kataoka, *Angew. Chem., Int. Ed.* **2003**, *42*, 4640. b) V. R. Sinha, A. Trehan, *J. Controlled Release* **2003**, *90*, 261. c) H. Tamber, P. Johansen, H. P. Merkle, B. Gander, *Adv. Drug Delivery Rev.* **2005**, *57*, 357.

3 a) A. N. Zelikin, Q. Li, F. Caruso, *Angew. Chem., Int. Ed.* **2006**, *45*, 7743. b) F. Caruso, D. Trau, H. Möhwald, R. Renneberg, *Langmuir* **2000**, *16*, 1485.

4 L. Dähne, S. Leporatti, E. Donath, H. Möhwald, *J. Am. Chem. Soc.* **2001**, *123*, 5431.

5 A. Wyss, J. Boucher, A. Montero, I. Marison, *Enzyme Microb. Technol.* **2006**, *40*, 25.

6 a) M. Grätzel, *Nature* **2001**, *414*, 338. b) W. U. Huynh, J. J. Dittmer, A. P. Alivisatos, *Science* **2002**, *295*, 2425.

7 S.-W. Kim, M. Kim, W. Y. Lee, T. Hyeon, *J. Am. Chem. Soc.* **2002**, *124*, 7642.

8 Z. Yang, Z. Niu, Y. Lu, Z. Hu, C. Han, *Angew. Chem., Int. Ed.* **2003**, *42*, 1943.

9 X. Wang, P. Hu, Y. Fangli, L. Yu, *J. Phys. Chem. C* **2007**, *111*, 6706.

10 H. T. Schmidt, A. E. Ostafin, *Adv. Mater.* **2002**, *14*, 532.

11 Z. X. Wang, M. Chen, L. M. Wu, *Chem. Mater.* **2008**, *20*, 3251.

12 a) T. Liu, Y. Xie, B. Chu, *Langmuir* **2000**, *16*, 9015. b) Y. Ma, L. Qi, J. Ma, H. Cheng, *Langmuir* **2003**, *19*, 4040.

13 a) M. Yang, J. Ma, C. L. Zhang, Z. Z. Yang, Y. F. Lu, *Angew. Chem., Int. Ed.* **2005**, *44*, 6727. b) M. Yang, J. Ma, Z. W. Niu, X. Dong, H. F. Xu, Z. K. Meng, Z. G. Jin, Y. F. Lu, Z. B. Hu, Z. Z. Yang, *Adv. Funct. Mater.* **2005**, *15*, 1523. c) Z. C. Wu, M. Zhang, K. Yu, S. D. Zhang, Y. Xie, *Chem.—Eur. J.* **2008**, *14*, 5346.

14 a) X. W. Lou, C. L. Yuan, L. A. Archer, *Small* **2007**, *3*, 261. b) H. L. Xu, W. Z. Wang, *Angew. Chem., Int. Ed.* **2007**, *46*, 1489. c) H. G. Zhang, Q. S. Zhu, Y. Zhang, Y. Wang, L. Zhao, B. Yu, *Adv. Funct. Mater.* **2007**, *17*, 2766.

15 a) J. Liu, H. Xia, D. F. Xue, L. Lu, *J. Am. Chem. Soc.* **2009**, *131*, 12086. b) Z. X. Wang, X. B. Chen, M. Chen, L. M. Wu,

Langmuir **2009**, *25*, 7646. c) J. J. Li, S. J. Ding, C. L. Zhang, Z. Z. Yang, *Polymer* **2009**, *50*, 3943.

16 R. B. Yu, L. Yan, P. Zheng, J. Chen, X. R. Xing, *J. Phys. Chem. C* **2008**, *112*, 19896.

17 R.-J. La, Z.-A. Hu, H.-L. Li, X.-L. Shang, Y.-Y. Yang, *Mater. Sci. Eng., A* **2004**, *368*, 145.

18 K. B. Zhou, Z. Q. Yang, S. Yang, *Chem. Mater.* **2007**, *19*, 1215.

19 G. Z. Chen, C. X. Xu, X. Y. Song, S. L. Xu, Y. Ding, S. X. Sun, *Cryst. Growth Des.* **2008**, *8*, 4449.

20 S. T. Kim, J. S. Lee, C. Mitterbauer, Q. M. Ramasse, M. C. Sarahan, N. D. Browning, H. J. Park, *Chem. Mater.* **2009**, *21*, 1182.

21 Z. Y. Guo, F. L. Du, G. C. Li, Z. L. Cui, *Inorg. Chem.* **2006**, *45*, 4167.

22 D. G. Zhang, Z. W. Tong, S. Z. Li, X. Zhang, A. Ying, *Eur. J. Inorg. Chem.* **2008**, 5476.

23 Z. Y. Guo, F. L. Du, Z. L. Cui, *Mater. Chem. Phys.* **2009**, *113*, 53.

24 a) C. Ho, J. C. Yu, T. Kwong, A. C. Mak, S. Lai, *Chem. Mater.* **2005**, *17*, 4514. b) C. W. Sun, J. Sun, G. L. Xiao, H. R. Zhang, X. P. Qiu, H. Li, L. Q. Chen, *J. Phys. Chem. B* **2006**, *110*, 13445.

25 M.-M. Titirici, M. Antonietti, A. Thomas, *Chem. Mater.* **2006**, *18*, 3808.

26 C.-Y. Chang-Chien, C.-H. Hsu, T.-Y. Lee, C.-W. Liu, S.-H. Wu, H.-P. Lin, C.-Y. Tang, C.-Y. Lin, *Eur. J. Inorg. Chem.* **2007**, 3798.

27 X. M. Sun, J. F. Liu, Y. D. Li, *Chem.—Eur. J.* **2006**, *12*, 2039.

28 Z. Y. Guo, F. F. Jian, F. L. Du, *Scr. Mater.* **2009**, *61*, 48.

29 F. Gao, Z. Xu, Q. Wang, Z. Hu, G. Gu, *J. Dispersion Sci. Technol.* **2009**, *30*, 178.

30 a) Z. J. Yang, L. Liu, H. Liang, H. X. Yang, Y. Z. Yang, *J. Cryst. Growth* **2010**, *312*, 426. b) Y. T. Song, J. J. Wei, Y. Z. Yang, Z. J. Yang, H. X. Yang, *J. Mater. Sci.* **2010**, *45*, 4158.

31 a) L. Vayssieres, K. Keis, S.-E. Lindquist, A. Hagfeldt, *J. Phys. Chem. B* **2001**, *105*, 3350. b) L. Vayssieres, K. Keis, A. Hagfeldt, S.-E. Lindquist, *Chem. Mater.* **2001**, *13*, 4395.

32 E. Paparazzo, G. M. Ingo, N. Zacchett, *J. Vac. Sci. Technol., A* **1991**, *9*, 1416.

33 H. L. Zhu, K. H. Yao, H. Zhang, D. R. Yang, *J. Phys. Chem. B* **2005**, *109*, 20676.

34 I. Shweky, A. Bino, D. P. Goldberg, S. J. Lippard, *Inorg. Chem.* **1994**, *33*, 5161.

35 S. Farhikhteh, A. Maghsoudipour, B. Raissi, *J. Alloys Compd.* **2010**, *491*, 402.

36 G. Vanhoyland, J. Pagnaer, J. D'Haen, S. Mullens, J. Mullens, *J. Solid State Chem.* **2005**, *178*, 166.

37 T. Masui, H. Hirai, N. Imanaka, G. Adachi, T. Sakata, H. Mori, *J. Mater. Sci. Lett.* **2002**, *21*, 489.

38 Y.-P. Liu, Y.-Y. Di, D.-H. He, Y.-X. Kong, W.-W. Yang, W.-Y. Dan, *J. Chem. Thermodyn.* **2010**, *42*, 513.

39 Y.-W. Zhang, R. Si, C.-S. Liao, C.-H. Yan, C.-X. Xiao, Y. Kou, *J. Phys. Chem. B* **2003**, *107*, 10159.

40 L. Brus, *J. Phys. Chem.* **1986**, *90*, 2555.

41 A. Trovarelli, *Catal. Rev.* **1996**, *38*, 439.